ERID 095717
RPF

Available online at www.sciencedirect.com
SCIENCE DIRECT
ELSEVIER
Journal of Contaminant Hydrology 82 (2006) 338–356
JOURNAL OF Contaminant Hydrology
www.elsevier.com/locate/jconhyd

Investigation of gas production and entrapment in granular iron medium☆

W. Kamolpornwijit, L. Liang *

Environmental Sciences Division, Oak Ridge National Laboratory, P.O. Box 2008, Oak Ridge, TN 37830-6036, USA

Received 29 April 2004; received in revised form 26 September 2005; accepted 3 October 2005
Available online 5 December 2005

Abstract

A method for measuring gas entrapment in granular iron (Fe^0) was developed and used to estimate the impact of gas production on porosity loss during the treatment of a high NO_3^- groundwater (up to ~10 mM). Over the 400-d study period the trapped gas in laboratory columns was small, with a maximum measured at 1.3% pore volume. Low levels of dissolved $H_2(g)$ were measured (up to 0.07 ± 0.02 M). Free moving gas bubbles were not observed. Thus, porosity loss, which was determined by tracer tests to be 25–30%, is not accounted for by residual gas trapped in the iron. The removal of aqueous species (i.e., NO_3^-, Ca, and carbonate alkalinity) indicates that mineral precipitation contributed more significantly to porosity loss than did the trapped gases. Using the stoichiometric reactions between Fe^0 and NO_3^-, an average corrosion rate of 1.7 mmol kg^{-1} d^{-1} was derived for the test granular iron. This rate is 10 times greater than Fe^0 oxidation by H_2O alone, based on H_2 gas production. NO_3^- ion rather than H_2O was the major oxidant in the groundwater in the absence of molecular O_2. The N-mass balance [e.g., $N_2(g)$ and NH_4^+ and NO_3^-] suggests that abiotic reduction of NO_3^- dominated at the start of Fe^0 treatment, whereas N_2 production became more important once the microbial activity began. These laboratory results closely predict N_2 gas production in a separated large column experiment that was operated for ~2 yr in the field, where a maximum of ~600 ml d^{-1} gas volumes was detected, of which 99.5% (v/v) was N_2. We conclude that NO_3^- suppressed the production of $H_2(g)$ by competing with water for Fe^0 oxidation, especially at the beginning of water treatment when Fe^0 is highly reactive. Depends on the groundwater composition, gas venting may be necessary in maintaining PRB performance in the field.
Published by Elsevier B.V.

Keywords: Gas production; Gas entrapment; Zero-valent iron technology; Nitrate reduction; Iron corrosion rate

☆ The submitted manuscript has been authored by a contractor of the U.S. Government under contract No. DE-AC05-00OR22725. Accordingly, the U.S. Government retains a nonexclusive, royalty-free license to publish or reproduce the published form of this contribution, or allow others to do so, for U.S. Government purposes.

* Corresponding author. Tel.: +1 865 241 3933; fax: +1 865 576 9977.
E-mail address: liangl@ornl.gov (L. Liang).

0169-7722/$ - see front matter. Published by Elsevier B.V.
doi:10.1016/j.jconhyd.2005.10.009

14697

1. Introduction

The operating life of zero-valent iron-based permeable reactive barriers (Fe^0-PRB) is affected by loss of both Fe^0 reactivity toward contaminant (Farrell et al., 2000; Vikesland et al., 2003) and media hydraulic conductivity; the latter can result from mineral precipitation (Mackenzie et al., 1999; Liang et al., 2000; Phillips et al., 2000; Kamolpornwijit et al., 2003; Morrison, 2003; Wilkin et al., 2003), bacteria accumulation (Gu et al., 1999), and gas production (Bokermann et al., 2000; Vikesland et al., 2003). The loss of chemical reactivity and mineral precipitation on system performance have been widely studied both in the laboratory (Mackenzie et al., 1999; Farrell et al., 2000; Kamolpornwijit et al., 2003; Klausen et al., 2003; Vikesland et al., 2003) and at field (Morrison and Cahn, 1991; McMahon and Sandstrom, 1999; Wilkin et al., 2003; Liang et al., 2005). Effects of gas production and entrapment on system hydraulics, in contrast, are poorly understood. Although gas can transport with water, residual bubbles, however, can become trapped in the porous media. Gas may vent naturally in an open system, e.g., a continuous wall configuration, via bubble coalescence and buoyant movement. In closed systems, e.g., treatment reactors of a funnel-and-gate configuration, a high rate of gas production and restricted venting could produce gas locks and potentially shut down the system (Birke, 2003).

Gas production in the Fe^0-PRB is expected from both chemical and microbial-mediated processes. Stoichiometrically, a mole of hydrogen gas [$H_2(g)$] is produced when a mole of Fe^0 is oxidized by water in the absence of O_2 [Eq. (1)] (Reardon, 1995). The absorbed hydrogen (H_{abs}) atoms resulting from Fe^0 reactions with carbonic acid and bicarbonate [Eqs. (2) and (3)] (McIntire et al., 1990) can subsequently combine and form H_2. The nitrate (NO_3^-) ions have been reported to increase the corrosion rate of Fe^0 via abiotic and biotic pathways (Huang et al., 1998; Till et al., 1998; Kamolpornwijit et al., 2003). Abiotic NO_3^- reduction [Eq. (4)] will produce ammonium ion (NH_4^+), which in turn may transform to ammonia gas [$NH_3(g)$] at pH>pKa [Eq. (5)] (Stumm and Morgan, 1996). The microbial mediated process [Eq. (6)] could convert two moles of NO_3^- to one mole of nitrogen gas [($N_2(g)$] as an end product (Till et al., 1998; Kielemoes et al., 2000). The microbial-mediated reduction of sulfate (SO_4^{2-}) also influences gas formation by consuming H_2 and potentially producing hydrogen sulfide gas [$H_2S(g)$] under acidic conditions [Eq. (7)] (Gu et al., 1999).

$$Fe^0 + 2H_2O = Fe^{2+} + H_2 + 2OH^- \quad (1)$$

$$H_2CO_3 + e^- = HCO_3^- + H_{abs} \quad (2)$$

$$HCO_3^- + e^- = CO_3^{2-} + H_{abs} \quad (3)$$

$$4Fe^0 + NO_3^- + 7H_2O = 4Fe^{2+} + NH_4^+ + 10OH^- \quad (4)$$

$$NH_4^+ = H^+ + NH_3 \quad (5)$$

$$5Fe^0 + 2NO_3^- + 6H_2O = 5Fe^{2+} + N_2 + 12OH^- \quad (6)$$

$$SO_4^{2-} + 4H_2 = S^{2-} + 4H_2O \quad (7)$$

Gas species produced from these reactions may be present as dissolved or nucleated gas

on the amount of dissolved gas vary widely. Low levels of dissolved H_2 gas have been measured in some laboratory and field studies (Vikesland et al., 2003; Wilkin et al., 2003), so did elevated $H_2(g)$ concentrations in groundwater containing SO_4^{2-} (Gu et al., 1999) and NO_3^- (Kielemoes et al., 2000), and in the field (Wilkin et al., 2003). In batch studies, H_2, both as dissolved and as free gas bubbles (measured by gas pressure), has been observed to change with time (Reardon, 1995; Bokermann et al., 2000). The large variability in the observed gas production may be attributed to the differences in aqueous chemistry (Reardon, 1995; Liang et al., 2000) and in some cases, system configurations (Birke, 2003).

Trapped gas replaces pore water, hence reduces residence time. Formation of H_2 film on iron grains has been suggested to contribute to the loss of porosity (Mackenzie et al., 1999; Kober et al., 2002). However, little is known on gas entrapment in Fe^0 media and its effects on the hydraulic performance because of difficulty in measuring the trapped gas volume. It is therefore the objective of this study to develop a method to quantify trapped gases and to test the following hypotheses: (1) substantial gas phase exists in Fe^0 media which causes porosity loss and in the worse case, stops flow; and (2) the presence of NO_3^- affects the mechanisms of gas production and specifically, denitrification may control gas generation. Groundwater from an existing PRB site (containing high levels of NO_3^-) was used in flow-through experiments. The results of gas volumes and speciation and aqueous speciation are discussed with respect to the mechanisms of gas production, Fe^0 corrosion, and porosity loss in Fe^0 medium over time.

2. Materials and method

Residual gas bubbles and their effects on the porosity loss were investigated by pumping an actual groundwater through packed columns of granular iron. Granular iron ranging from 8 to 50 mesh size was obtained from Peerless Industry. The study was initiated a year after the onset of a field column study (Kamolpornwijit et al., 2003), where large volumes of free and trapped gases were observed after 6-month operation. Although routine measurements were made subsequently, data were not collected on gas entrapment during the initial operation of the field columns. Thus the bench top columns were set up in the laboratory to observe gas production during the initial stage of Fe^0 treatment and to supplement data to the field column study.

2.1. Groundwater source

The groundwater used in the laboratory was collected from the same well as for the field column study, which is located ~70 ft upgradient of an existing PRB (See Fig. 1 in Liang et al., 2005) at the Y-12 National Security Complex, Oak Ridge, Tennessee. The site groundwater contained high levels of NO_3^- (up to 10 mM) and total dissolved solid (TDS) (Table 1). A 10-l Tedlar® bag was used to collect groundwater and was refilled weekly. The holding bags maintained the groundwater reasonably well, although some changes in pH (6.67 to 6.87) and alkalinity (296 to 298 ppm as $CaCO_3$) were observed after 3 days. Gas bubbles were observed on the surface of the holding bags, presumably from CO_2 degassing due to a decrease in the hydrostatic pressure of the well water. This weekly variation, however, was small compared to the temporal and seasonal changes in the site groundwater (see the major constituents of the groundwater in Table 1).

Groundwater, with relatively low levels of TDS, alkalinity, and NO_3^-, was also used in the period of 153 to 181 d to study H_2 production from anaerobic Fe^0 oxidation by water. During

Table 1
Chemical characteristics of influent groundwater, with concentrations in mM unless otherwise noted

Parameters	Influent		Recirculation
	Range	Average[a]	Average
pH	6.71–7.61	6.947	6.625
Total alkalinity (mEq)	1.64–3.26	2.321	0.165
Conductivity (ms/cm)	1.02–1.96	1.798	1.295
Dissolved O_2	0.01–0.02	0.015	NA
NO_3^-	1.82–10.40	8.822	5.44
SO_4^{2-}	0.47–0.84	0.545	0.70
Cl^-	0.59–2.12	1.775	2.47
Ca	4.09–8.31	7.377	2.6
Fe	0–0.003	0.0003	0.046
Mg	0.85–0.95	0.871	0.868
Si	0.06–0.08	0.065	0.012
Al	0.00–0.02	0.006	0.012
Mn	0.00–0.02	0.012	0.006
Na	0.27–0.94	0.393	0.476

[a] Time-weighted average.

back into the columns. The influent composition during the recirculation period is shown in Table 1.

2.2. Column setup

Two borosilicate glass columns (SMC1 and SMC2), with 4.8-cm inside diameter and 30-cm length, were setup vertically in the laboratory (Fig. 1). Iron grains were wet-packed into the columns using the test groundwater. Well graded #4 sands were added to the columns to 3-cm depth at both inlet and outlet ends to allow a better flow distribution. The grains were slowly added to the columns to minimize air entrapment. Tapping was applied for every cm of added grains to pack the medium. The porosities of the packed columns were 57.1% and 61.1%, respectively, calculated using the bulk density and the weight changes before and after packing. The mass of packed Fe^0 for both columns was ~1.46 kg.

Infusion pumps (AVI 200A, 3M, Infusion Therapy, St. Paul, MN) were used to pump upward the air-free groundwater to both columns. The flow rates were set at ~14 ml h^{-1}, equivalent to a pore velocity of ~0.31 m d^{-1}. This yielded an initial residence time of ~23 h. The vertical mounting of the columns was to better control flow, to increase the path of gas movement, and to allow gas venting; thus closely simulating the field conditions of PRB. The flow direction of water may artificially increase gas venting. However, free gas bubbles were not observed in the effluent discharge line at any time during the course of the experiment.

Two separate control experiments (C1 and C2) were also conducted to estimate the trapped air volume in the column assembly. In experiment C1, only groundwater was present in the column, whereas in C2, column was wet-packed with sand. The sand packed column may not be an ideal control for the granular iron column, nonetheless it served as a baseline for potential trapped gas volume during packing.

Contrast to the laboratory columns, groundwater flowed horizontally in the field columns. The vertical path of gas movement was of a maximum 15.2-cm, compared to the 30-cm in the laboratory columns. Two flow rates were used in the field column study, one initially set at

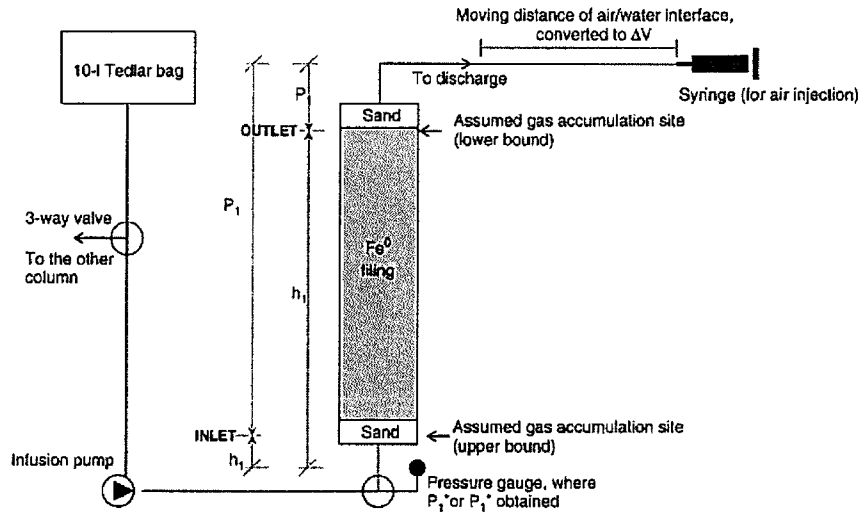

Fig. 1. Laboratory column setup, with schematics for trapped air quantification. P_1^* and P_2^* are pressure heads registered at the pressure gauge; P_1^* is taken under atmospheric pressure and P_2^* is taken under external pressure (ΔP) corresponding to movement of air/water interface caused by air injection. P_1 is pressure head imparted on trapped gas, which equals to $P_1^* - h_1$. The potential heads, h_1 vary with the assumed location of gas accumulation. The 10-l Tedlar bag was used as the groundwater reservoir.

d^{-1}), both were controlled using HPLC pumps. This high flow rate was used to increase the throughput, thus allowing observation of Fe^0 corrosion due to large volume treatment in a short time frame. Gases were vented regularly through multiple vent ports located at the upper boundary of the columns (Kamolpornwijit et al., 2003). During the initial period, gas volume was not measured.

About 6-month into the field study, the observed residence time decreased from the initial values. A routine measurement of gas production was implemented and the vented free gas was substantial. It was hypothesized that loss of porosity was caused in part by accumulation of trapped gas. To test the hypothesis, a simple procedure was developed to extract gas from the columns and observe the restoration of porosity. Trapped gas was slowly extracted from the vent port under no flow conditions using gas tight syringe partly filled with groundwater. The removal of gas induced a slight negative pressure which was brought back to atmospheric pressure by injection of the pre-filled groundwater in the syringe. This procedure was planned for the laboratory study when gas production becomes high, with an aim to differentiate the porosity loss due to mineral precipitates from gas entrapment.

2.3. Sampling and analysis

2.3.1. Water sample

Both influent and effluent samples were analyzed for cations, anions, and other water quality parameters, such as pH and dissolved oxygen. Dissolved metals, such as Ca, Mg, Fe, Si, Na, and K, were analyzed using ICP (Thermo Jarrell Ash ICAP OES) and Fe^{2+} was

SO_4^{2-}, were analyzed using IC (Dionex120); S^{2-} was analyzed by methylene blue method (Chemetric®); and NH_4^+ using a NH_3 probe (Orion 9512 NH_3 gas sensing electrode with NH_3–pH adjusting ISA). Alkalinity was determined by titration with a standard HCl solution to 4.5. The effluent samples were collected in a Tedlar bag, usually overnight. The pH probe was calibrated before inserting it into the effluent line and a measurement was taken when a steady reading was obtained.

2.3.2. Tracer test

Tracer tests were conducted periodically for both columns. A concentrated KBr solution was pre-mixed with the groundwater to make a Br^- solution of 1000 ppm. The Br^-containing groundwater was then injected at the same flow rate for 2.5 h. The effluent was collected every 45 min using an auto-sampler (Spectra/Chrom CF-1 fraction collector) over a period of 3 d. Bromide concentration in the effluent was analyzed using an IC.

2.3.3. Dissolved gas analysis

The concentration of dissolved gas was obtained using a head-space analysis at gas/water equilibrium. Known volumes (~210–250 ml) of effluent samples were collected over night in a Tedlar bag, which had been flushed with He or Ar gas several times and filled with 100-ml of the corresponding gases. Helium was used in gas collection for GC analysis with a TCD, and Ar for MS analysis. After sample collection, the sealed sample bags were mixed on a shaker for about 2 h to allow the gas to reach equilibrium with water. A gas sample was drawn from the headspace and was then analyzed.

2.3.4. Quantification of trapped gas

Assuming an ideal gas behavior for the trapped gas within the column, the gas volume can be calculated based on its compressibility:

$$V_1 = P_2(\Delta V)/(\Delta P). \tag{8}$$

Where V_1 is the gas volume under pressure P_1, and ΔV is the change in gas volume that caused by the change of pressure (ΔP) from P_1 to P_2. Experimentally, the pressures and gas volumes were determined under no flow conditions. The measurement normally took less than 30 min during which the flow in the columns was temporarily shut off. The first pressure reading (P_1^*) was taken with effluent open to atmospheric pressure. A volume of air was then injected into the effluent line using a gas-tight syringe creating a pressure change, ΔP. The injection pushed the water (in the effluent tube) toward the column and the water/air interface moved a specific distance (Fig. 1), which was converted to the replacement volume, ΔV. The observed pressure at the pressure gauge, P_2^* ($=P_1^*+\Delta P$) was recorded. Here, we assumed that the liquid is incompressible. The gas injection was always done within the length of effluent tubing, i.e., the injected air had never gone into the column.

Note that the pressure gauge was installed upgradient of the column inlet, not at the point of gas accumulation (Fig. 1). Therefore, pressure gauge readings (i.e., P_1^* and P_2^*) need to be corrected for the location of gas accumulation prior to their substitution as P_1 and P_2 in Eq. (8). For example, $P_1=P_1^*-h_1$ (Fig. 1), where h_1 is the potential head (or height) of the assumed location of gas accumulation referenced to the pressure gauge. The accumulation location cannot be precisely identified. By assigning location of gas entrapment, two limits of trapped gas volumes are estimated: the upper limit is obtained when gas is accumulated at the column inlet,

When trapped gas is assumed to distribute uniformly across the column, the volume is calculated by Eq. (9). The integrated form of Eq. (9) is provided in Eq. (10):

$$V_1 = \frac{\Delta V}{\Delta P} \int_{h_{in}}^{h_{out}} \frac{(P_2^* - h)}{L} dh \tag{9}$$

$$V_1 = \frac{\Delta V}{\Delta P} \left(P_2^* - \frac{h_{out} + h_{in}}{2} \right). \tag{10}$$

Where L ($=h_{out} - h_{in}$) is the length of the column, h is the potential head of the location of gas entrapment referenced to the pressure gauge, h_{in} is potential head at the column inlet, and h_{out} is at the column outlet. The calculated volume lies within the two limiting values.

2.3.5. Quantification of free gas

Since free gas bubbles were not observed from laboratory columns, the procedure applied only to the field study. A series of Tedlar bags that were pre-filled with a small amount of groundwater were attached to column venting ports. After a given period time of collection, the bags were detached from the columns. Gas vented into the bags was quantified by slowly extracting it into a gas tight syringe until the bag was depleted of gas. Adding small volume of groundwater in Tedlar bags facilitated gas measurement and reduced artificial error from an excessive application of negative pressure.

3. Results and discussion

3.1. Entrapped gas volumes and dissolved gas speciation

The gas entrapment in Fe^0 media was listed and plotted as trapped gas volumes over time in Table 2 and Fig. 2, respectively. The effluent pH values were also plotted. The results from the two columns (SMC1 and SMC2) show similar trends although the absolute values differ slightly. Since $H_2(g)$ production at a corroding Fe^0 surface is a sporadic process, the disparity is expected (Reardon, 1995). Using the results from SMC1, 1.8-ml volume of trapped gas was obtained on the 2nd d of the operation (Fig. 2). This result was based on a uniform distribution of gas within the column and equivalent to 0.7% of the total Fe^0 pore volume (pv=260 ml). The upper and lower limits of trapped gas volumes were calculated for SMC1 (Table 2), which show similar trend. Residual gas bubbles were visibly found near the column outlets, potentially from the buoyancy forces. This is consistent with the field column observations where gases mainly accumulated at the crowns of the horizontal columns and near the outlets. Note that trapped gas volumes presented in Table 2 are 'as measured', not corrected for the control.

The gas production and entrapment varied with time (Fig. 2). During the initial period of <75 d, the trapped gas volume fluctuated from 1.4 to 3.5 ml (0.5–1.3% pv). After reaching the peak value of 3.5 ml on 31 d, the trapped gases showed a decreasing trend. A continuous decrease in gas volume occurred from 75 to 171 d. Thereafter, gas volume slowly built up. From ~293 d, it increased significantly, reaching 3.2 ml by 318 d. Overall, the trapped gas volume was small, with a maximum value of ~3.5 ml, equivalent to 1.3% pv. Unlike the significant degassing observed in studies where NO_3^- was absent (Liang et al., 1996; Vikesland et al., 2003), free-moving gas bubbles were not observed in the effluent during the

Table 2
Estimated gas volumes for SMC1 based on measured pressure head values and air replacement volumes

Run time (d)	P_1^* (in)	P_2^* (in)	ΔV^a (ml)	Estimated gas volume[b] (ml)		
				Gas trapped at outlet, $h_1=12$ in	Gas trapped at inlet, $h_1=2.5$ in	Uniform distribution
2	24	36	0.79	1.57 ± 0.03	2.20 ± 0.08	1.80 ± 0.05
3	27	38	0.87	2.06 ± 0.06	2.81 ± 0.13	2.34 ± 0.08
9	25	39	0.74	1.44 ± 0.03	1.94 ± 0.07	1.62 ± 0.04
10	25	45	0.78	1.27 ± 0.02	1.64 ± 0.04	1.41 ± 0.02
20	24	37	0.76	1.47 ± 0.03	2.03 ± 0.07	1.67 ± 0.04
21	23	35	0.76	1.46 ± 0.03	2.07 ± 0.07	1.69 ± 0.04
23	24	33	0.77	1.79 ± 0.05	2.60 ± 0.13	2.09 ± 0.08
27	25	31	0.77	2.25 ± 0.09	3.38 ± 0.25	2.67 ± 0.14
31	26	31	0.77	2.93 ± 0.18	4.39 ± 0.46	3.46 ± 0.26
35	25	32	0.77	2.20 ± 0.09	3.24 ± 0.23	2.58 ± 0.13
36	25	32	0.77	2.20 ± 0.09	3.24 ± 0.23	2.58 ± 0.13
42	24	33	0.77	1.80 ± 0.02	2.61 ± 0.13	2.10 ± 0.08
52	24	35	0.77	1.65 ± 0.02	2.35 ± 0.10	1.91 ± 0.06
72	24	39	0.77	1.39 ± 0.02	1.87 ± 0.06	1.57 ± 0.03
78	24	29	0.77	2.62 ± 0.13	4.08 ± 0.39	3.16 ± 0.21
80	25	31	0.77	2.25 ± 0.09	3.28 ± 0.25	2.67 ± 0.14
111	24	40	0.77	1.35 ± 0.02	1.80 ± 0.05	1.52 ± 0.03
114	24	45	0.78	1.19 ± 0.01	1.54 ± 0.03	1.32 ± 0.02
129	24	40	0.48	0.85 ± 0.01	1.14 ± 0.03	0.95 ± 0.02
133	25	42	0.48	0.86 ± 0.01	1.13 ± 0.03	1.96 ± 0.02
136	25	87	0.69	0.84 ± 0.00	0.94 ± 0.01	0.88 ± 0.01
146	25	126	0.69	0.78 ± 0.00	0.85 ± 0.00	0.81 ± 0.00
150	25	135	0.69	0.77 ± 0.00	0.83 ± 0.00	0.80 ± 0.00
171	25	82	0.26	0.32 ± 0.00	0.36 ± 0.00	0.33 ± 0.00
181	25	155	0.69	0.76 ± 0.00	0.81 ± 0.00	0.78 ± 0.00
258	25	56	0.73	1.04 ± 0.01	1.26 ± 0.02	1.12 ± 0.01
287	25	52	0.73	1.08 ± 0.01	1.34 ± 0.02	1.18 ± 0.02
293	24	38	0.73	1.36 ± 0.02	1.86 ± 0.06	1.54 ± 0.04
297	24	36	0.73	1.46 ± 0.03	2.04 ± 0.08	1.68 ± 0.04
308	25	32	0.78	2.23 ± 0.09	3.29 ± 0.23	2.62 ± 0.13
311	27	39	0.78	1.76 ± 0.05	2.38 ± 0.10	1.99 ± 0.07
318	25	28	0.49	2.61 ± 0.25	4.16 ± 0.74	3.18 ± 0.40
325	26	31	0.59	2.26 ± 0.14	3.38 ± 0.36	2.67 ± 0.20
342	26	30	0.55	2.49 ± 0.19	3.81 ± 0.51	2.98 ± 0.29
C1[c]	39	131	0.24	0.25 ± 0.00	0.29 ± 0.00	0.27 ± 0.00
C2[d]	39	114	0.39	0.42 ± 0.00	0.49 ± 0.01	0.45 ± 0.00

Note: P_1^* and P_2^* are pressure head readings at the pressure gauge; P_1^* is taken under atmospheric pressure and P_2^* is taken under external pressure (ΔP) corresponding to movement of air/water interface caused by air injection.
The average values based on a uniform distribution are plotted in Fig. 2.

[a] ΔV — replacement volume, calculated from the moving distance of the water/air interface in the effluent tube with a cross-sectional area of 0.0198 cm^2 (Fig. 1).

[b] Trapped gas volume calculated for the assumed location of accumulation, using Eqs. (8) and (10), where P_1 and P_2 are the pressure heads imparted on trapped gas, relating to P_1^* and P_2^* as follows: $P_1=P_1^*-h_1$, $P_2=P_2^*-h_1$ and $\Delta P=P_2-P_1$. No correction for the volumes from C1 and C2 was made.

[c] A control experiment for columns filled with water only.

[d] A control experiment for columns filled with water and sand.

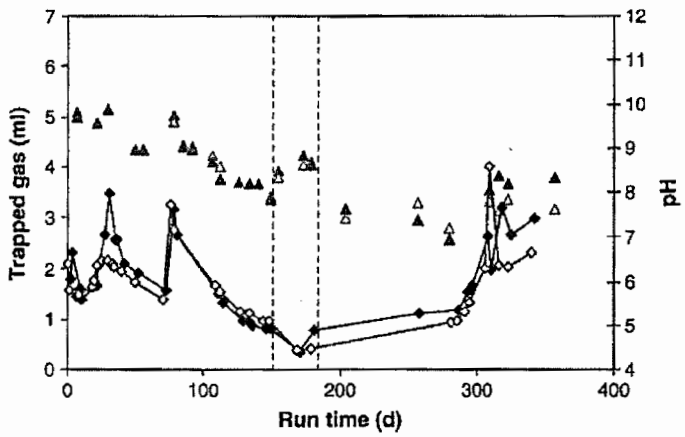

Fig. 2. Trapped gas volumes and pH in the laboratory columns. The filled (◆) and open (◇) diamonds represent gas volumes estimated based on a uniform distribution for columns, SMC1 and SMC2. The filled (▲) and open (△) triangles represent the effluent pH values. Dashed lines mark a period when the effluent was recirculated back into the columns.

Because free gas was not produced in the study, dissolved gases were analyzed for gas speciation. At gas/water equilibrium, the distribution of dissolved gas may reflect the composition of the residual gas bubbles trapped in the medium. Like gas volumes, gas composition also varied with time (Table 3). On 22-d dissolved H_2 in the column effluents was measured at 0.07 ± 0.02 mM; thereafter, it was under detection limit (Table 3). On the later sampling dates, N_2 and CO_2 were the major gas species, with <20 μM dissolved O_2, and non-detectable NH_3.

Table 3
Dissolved gas concentrations in laboratory and field columns

Run time (day)			Gas species		
			H_2	N_2	CO_2
Henry's constant M/atm[a] →			0.00078	0.00061	0.032
Laboratory columns mM[b]	22[c]	SMC1	0.069	NA	NA
		SMC2	0.068	NA	NA
	234[d]	SMC1	BD	0.716	0.111
		SMC2	BD	0.91	0.002
	372[d]	Influent	BD	0.64	1.825
		SMC1	BD	0.347	0.175
		SMC2	BD	0.765	0.107
Field columns [e]	664[d]	Gas phase	<0.001%	99.5%	0.01%
		Aqueous phase	BD	0.607	0.0003

[a] From Wilhelm et al., 1997.
[b] Headspace analysis after equilibrium with aqueous phase (see section Dissolved gas analysis).
[c] Analysis obtained with TCD.
[d] Analysis obtained with MS. BD signifies below detection.
[e] Gas phase analysis presented in % of total gas. The aqueous phase concentration in mM was calculated based on

3.2. Mechanisms of gas production on the basis of chemical speciation

Gases in Fe^0 packed columns are composed of mainly (1) H_2 resulting from Fe^0 corrosion by water, (2) NH_3 and N_2 from reduction of NO_3^-, and (3) CO_2 from degassing and partitioning of influent groundwater. The changes in reaction mechanisms can influence the dynamics of gas production and speciation as we observed in this study. In the absence of molecular O_2, the oxidative action of H_2O alone will corrode Fe^0 at a rate of 0.4 mmol kg^{-1} d^{-1} (Reardon, 1995), which would produce 7.8 ml d^{-1} of gas [Eq. (1)] in our laboratory columns. This large quantity of gas should have been observed after a week of column operation on the basis that it took 70–200 h to reach a steady state in a batch reactor (Reardon, 1995). Gas production, in contrast, was sluggish in our study during treatment of groundwater containing 1.8–10.4 mM NO_3^- (Fig. 2). The maximum trapped gas was ~4 ml, with dissolved H_2<0.07 mM. At this concentration, equivalent to ~9% of the H_2 saturation level (0.78 mM), free H_2 bubbles are not expected.

Aqueous and dissolved gas speciation shows that the major reaction products are NH_4^+ (Fig. 3e) and N_2 (Table 3) in our treatment system. Selected aqueous chemical parameters, i.e., pH, NO_3^-, Ca, alkalinity, and NH_4^+ are shown in Fig. 3. The variation in the influent NO_3^- concentration reflected the temporal changes of the groundwater collected from the field site (Fig. 3c). However, after 100 d, the influent concentration maintained at ~9.7 mM except on 180 d when recirculation of low-NO_3^- water was performed. The average removal was ~1.8 mM and the highest NO_3^- removal was observed on 80 d, corresponding to a relatively low influent NO_3^- (Fig. 3c). Nitrate reduction may go through two different pathways, abiotic and biotic reaction according to Eqs. (4) and (6), respectively (Huang et al., 1998; Till et al., 1998; Kielemoes et al., 2000; Schlicker et al., 2000; Huang et al., 2003). The N-balance, based on the NH_4^+ production over NO_3^- removal, fluctuated between ~120% at the beginning of the experiment and ~60% at the end of the experiment (Fig. 3e). Before 300 d, NH_4^+ production could account for the loss of NO_3^-, which suggest that abiotic NO_3^- reduction [Eq. (4)] was the main mechanism (Hansen et al., 2001; Devlin et al., 2002; Westerhoff and James, 2003).

Ammonium was not present in the influent. Although ~1.8 mM of NO_3^- was converted to NH_4^+ the high solubility of NH_3 may not favor free NH_3 gas in the porous medium. Chemical equilibrium favors NH_3 [Eq. (5)] only at pH>pKa of 9.26, (Stumm and Morgan, 1996), a condition that may allow free NH_3 gas to evolve. Before 75 d trapped gas volume (Fig. 2) increased with pH, suggesting that NH_4^+ partition into NH_3 gas may be important. However, assuming aqueous–gas equilibrium in the columns, the calculated ratio of $NH_3(g)$ to total $NH_{3,T}$ [$=NH_4^+ + NH_3(a) + NH_3(g)$] was at best 0.13%, independent of the pH. With a complete conversion of 1.8 mM NO_3^- to NH_4^+, the maximum dissolved $NH_3(g)$ [0.0023 mM] is small compared to its Henry's law constant of 58 M atm^{-1} (Chameides, 1984). Thus on macroscopic scale, both NH_3 and H_2 gases are undersaturated, which will not produce free gas phase. The presence of residual free gas suggests that localized disequilibrium may exist, allowing gas nucleation and entrapment following NH_3 and H_2 production.

Toward the end of column experiments, the molar ratios of effluent NH_4^+ to the loss of NO_3^- show a discrepancy: only ~60% of NO_3^- was accounted for by NH_4^+ (Fig. 3e). Dissolved gas analysis show that N_2 was the major component (see results on 234 and 372 d in Table 3) and the concentrations were near to or higher than the aqueous saturation level. The facts that (1) N_2 emerged as the dominant dissolved gas, (2) a greater molar imbalance occurred between NH_4^+ and NO_3^- (see data>270 d in Fig. 3e), and (3) gas volume showed increasing trend (Fig. 2) as experiment progressed with time signify that denitrification of NO_3^- to N_2 became an additional

The fact that NH_4^+ and N_2 rather than H_2 were the major products suggests that NO_3^- reduction dominated that of H_2O in this treatment system. As a strong oxidant (Stumm and Morgan, 1996), NO_3^- could compete with H_2O for preferential reduction by Fe^0. Whether NO_3^- ions compete with H_2O molecules for Fe^0 surface sites, as proposed for nitrobenzene (Scherer et al., 2001) or use H_{abs} for their reduction is unknown (Bokermann, personal communication). The presence of NO_3^- in groundwater, however, appears to suppress H_2 gas production.

The influent groundwater contained high levels of dissolved CO_2, which could partition into the gas phase when pressure is reduced. In our experiments, column degassing was minimized by placing both influent bag and effluent discharge line slightly above the columns. However,

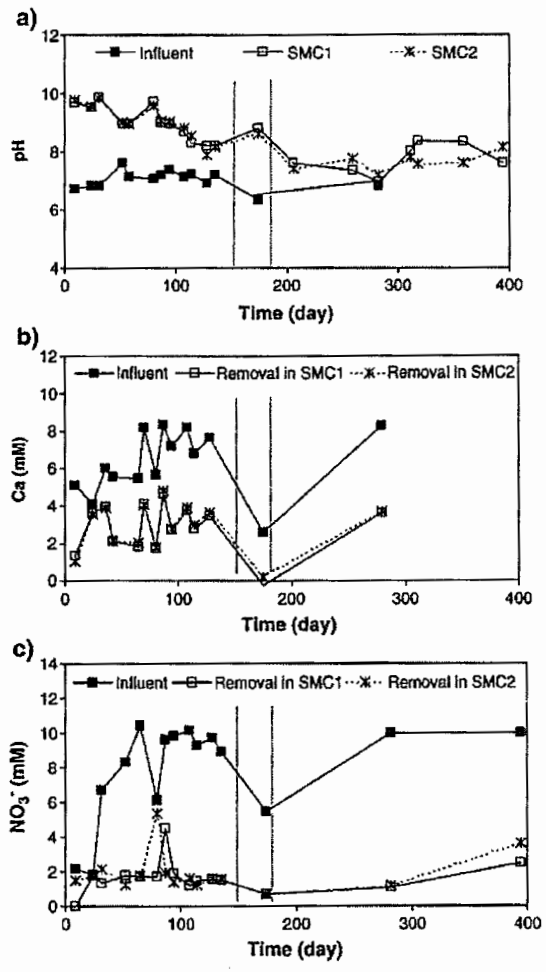

Fig. 3. Influent chemical parameters are plotted with changes in effluent over time: (a) effluent pH, (b) Ca removed from effluent, (c) NO_3^- removed from effluent (d) alkalinity removed from effluent, (e) the molar ratios of effluent NH_4^+ to the

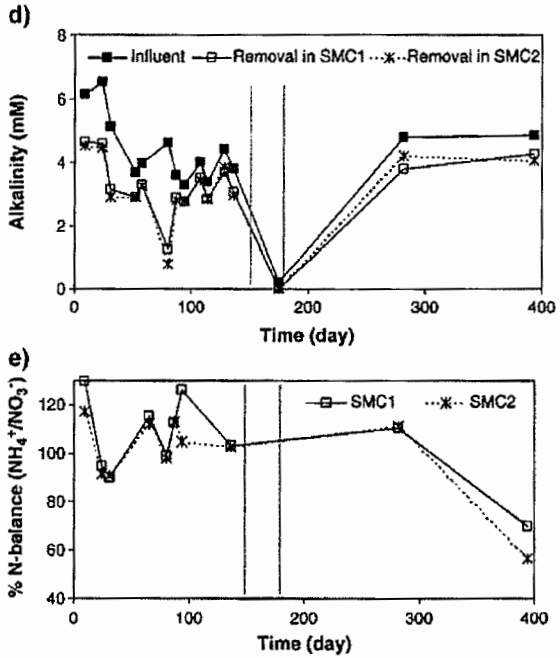

Fig. 3 (*continued*).

CO_2 gas measured at gas/aqueous equilibrium was lower in the effluent than in the influent (see 372 d in Table 3). This decrease in CO_2 gas was mainly caused by equilibrium speciation to HCO_3^- or CO_3^{2-} at pH>8 (Fig. 3a). Under this condition, $CaCO_3$ can become supersaturated and precipitate. Indeed, Ca^{2+} and carbonate alkalinity were both removed from the effluent (Fig. 3b and 3d, respectively), following a stoichiometric $CaCO_3$ precipitation. The molar differences between Ca and CO_3^{2-} were mostly within 10% to 25% and the discrepancy occurred during the initial period and when there was abnormal high rate of nitrate reduction. Ca adsorption at pH>8 (Yabusaki et al., 2001) and/or precipitation of siderite, carbonate green rust, or iron hydroxide carbonate (Phillips et al., 2000; Wilkin et al., 2003; Vikesland et al., 2003; Kamolpornwijit et al., 2004) may contribute to the observed discrepancies.

3.3. Iron corrosion and gas production

In the absence of dissolved O_2 (the influent dissolved oxygen was low throughout the study at ~15 μM, Table 1), Fe^0 may corrode through anaerobic oxidation by H_2O [Eq. (1)], reduction of NO_3^- (through both abiotic and biotic pathways [Eqs. (4) and (6)]), microbial-mediated reduction of SO_4^{2-} [Eq. (7)], and reaction with bicarbonate and carbonic acid [Eqs. (2) and (3)]. Using dissolved H_2 concentrations, rate of Fe^0 corrosion via anaerobic oxidation by H_2O was calculated to be <0.15 mmol kg^{-1} d^{-1}, which is much smaller than previous studies (Reardon, 1995). During the experimental periods, SO_4^{2-} and Cl^- remained at the same levels as the

play a role in gas production and Fe^0 corrosion in the current study, in contrast to previous work where test solution SO_4^{2-} was high (Gu et al., 1999). HCO_3^- and CO_3^{2-} species can promote Fe^0 corrosion via reactions shown in Eqs. (2) and (3) (McIntire et al., 1990). For example, with 0.02 M $NaHCO_3^-$, the corrosion rate was 1.5 times of a base-line value of 0.4 mmol kg^{-1} d^{-1} (Reardon, 1995). The carbonate alkalinity in the influent varied from ~4 to ~6 mEq (Fig. 3d), less than a half used in the previous study. Even if carbonate species exert influence on Fe^0 corrosion, the effect is relatively minor compared to that of NO_3^-.

Nitrate removal averaged at ~1.8 mM in the column study (Fig. 3c). Assuming stoichiometric reactions between Fe^0 and NO_3^- [Eqs. (4) and (6)], the corrosion rates of 1–4 mmol kg^{-1} d^{-1} were estimated (Kamolpornwijit et al., 2004). During the period of 153 to 181 d, the effluent was recycled back into the columns to observe the effect of relatively low levels of Ca, NO_3^- and alkalinity on iron corrosion and gas production (Two dotted lines are used to mark this period in Fig. 3). The temporary recirculation caused changes in effluent pH and Fe^0 corrosion, but did not significantly enhance H_2 gas production. In this period, the residual NO_3^- was still quite high (~6 mM). Excluding the corrosion rate during the recirculation period (~0.6 mmol kg^{-1} d^{-1}), the time-weighted corrosion rate was averaged at ~1.7 mmol kg^{-1} d^{-1} (~10 times higher than the rate based on H_2 production).

Obviously, unless the precise mechanisms involved in NO_3^- removal are known, the use of Eq. (4) or (6) to describe the removal of NO_3^- will predict significant differences in gas production. The composition and timing of the reaction products, e.g., NH_4^+ and N_2, suggest that the abiotic reduction accounted for most of NO_3^- removal prior to ~270 d and thereafter, denitrification became important, converting NO_3^- to N_2. In the study period, the influent pH was near neutral while the effluent pH increased to ~10 during the first 30 d, then decreased to ~8 near 120 d, and fluctuated at ~8 to the end of the experiment (Fig. 3a). This decreasing pH trend signifies a reduced Fe^0 reactivity and increased mineral precipitation because pH reflects the collected effects of OH^- production due to NO_3^- and H_2O reduction (Reardon, 1995; Till et al., Kielmose et al) and H^+ release due to mineral precipitation (Cornell and Schwertmann, 1996). It is also important that when pH is maintained at <9 the growth of microbial denitrifier can be sustained (Till et al., 1998). By the end of this study, the majority of NO_3^- reduction was still abiotic (>60%). Till et al. (1998) and Kielemoes et al. (2000) suggested that the biotic reduction of NO_3^- cannot compete with abiotic reduction unless the surface area and/or reactivity of the metallic iron is greatly reduced.

3.4. Gas production in the field column

Free gas volumes collected from the two field columns are plotted for the period of 200 d to the end of column operation, ~700 d (Fig. 4). The NO_3^- removal was also plotted. The volumes of the free gas reached a maximum of ~660 ml d^{-1} (equivalent to 6.6% of the initial pv of 10 l) in the high-flow column. In contrast, gas production in the low-flow column was much lower, with a maximum volume of ~50 ml/d (<1% of the initial pv). The vented free gas was composed of N_2 mainly, at 99.5%, with 0.01% CO_2 (Table 3). The NH_4^+ measured on 331-d accounted for ~20% NO_3^- removal in the two field columns (data not shown). The fact that the abiotic reduction of NO_3^- to NH_4^+ only partially accounted for NO_3^- removal and the fact that N_2 was prevalent in gas phase suggest that the gas production was predominantly microbially mediated. The onset of microbial activity requires an inoculation period and favorable pH to sustain the growth of denitrifier (Till et al., 1998), which explains the observation of increased N_2 gas

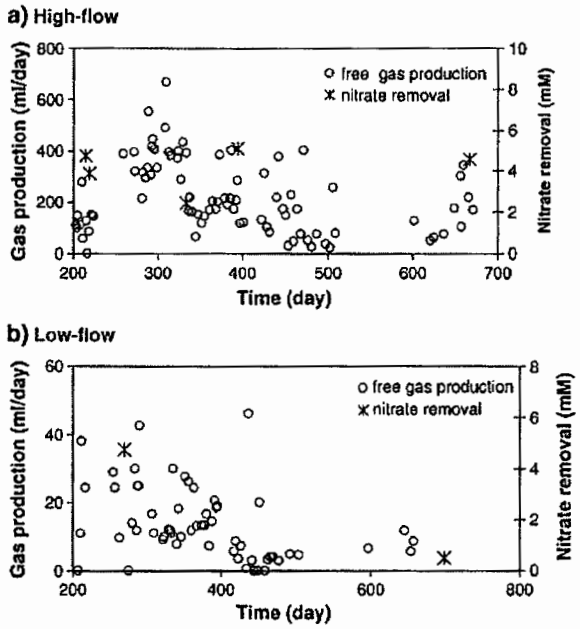

Fig. 4. Gas production and NO_3^- removal in field columns at run time > 200 d: (a) in high-flow column, with pore velocity of 1.2–1.7 m/d during the operation period. (b) in low-flow column, with pore velocity of 0.2–0.32 m/d.

Because reduction of NO_3^- to N_2 requires a transfer of 10 electrons, while only 2 are required for H_2 production, for the same extent of Fe^0 oxidation, NO_3^- reduction will produce a smaller amount of gas than will water under a steady state condition. Using the laboratory results of the corrosion rates (1–4 mmol kg^{-1} d^{-1}) and the flow characteristics of the columns, N_2 gas production was predicted (Table 4).

For the high-flow field column the estimated N_2 gas production varied from 0 to ~500 ml d^{-1}, the larger volume corresponds to the higher corrosion rate. These results agreed with the observed data range in Fig. 4. The variation in actual observation may reflect unsteady state condition, localized gas nucleation and other controls on gas movement (Fry et al., 1997; Mackenzie et al., 1999; Vikesland et al., 2003). For the low-flow column, which had a longer residence time, the steady state calculation predicts 0–80 ml d^{-1} gas production. These results are again in general agreement with the field observation (Fig. 4b), although the field data are more sporadic. The average observed rate of 20 ml d^{-1} is close to the prediction based on a corrosion rate of 2 mmol kg^{-1} d^{-1}. Using an average of 1.7-mmol kg^{-1} d^{-1} rate of corrosion, calculation shows that the laboratory column could produce 3.1 ml d^{-1} N_2. A rising trend in trapped gas volumes was observed at > 270 d (Fig. 2), but free gas bubbles were not observed.

3.5. Column hydraulics

During the 400-d operation of the laboratory columns, only a small quantity of trapped gas was detected (Fig. 2). The initial plan was to study effects of gas entrapment on the hydraulic

Table 4
Estimation of steady state free N_2 gas in the effluent due to denitrification

Run time (d)	Flow rate, Q[a] (ml d^{-1})	Pore velocity (cm d^{-1})	Residence time, τ (d)	Corrosion rate, k (mmol kg^{-1} d^{-1})	$[N_2]_T$[b] (mM)	$N_2(g)$[c] (mmol d^{-1})	Gas volume (ml d^{-1})
High-flow column							
400–500	14400	131.6	0.58	1.0	0.51	0	0
				2.0	1.01	5.80	141.8
				3.0	1.52	13.09	320.0
				4.0	2.03	20.39	498.2
Slow-flow column							
400–500	2160	19.7	1.54	1.0	0.54	0	0
				2.0	1.08	1.02	24.83
				3.0	1.62	2.18	53.34
				4.0	2.16	3.35	81.86
Laboratory column							
200–350	336	30.95	0.78	1.7	0.98	0.12	3.1

Field columns had 15-cm inside diameter and effective cross-sectional area of 109 cm^2, whereas the laboratory column had a cross-section of 10.9 cm^2. The iron path lengths were 76.2, 30.5 and 24 cm for high-, low-flow field and laboratory columns, respectively.

[a] Flow rates varied in experiments and an average is given for the period indicated.

[b] The total concentration of nitrogen is calculated by $[N_2]_T = 1/5\ (k \cdot \tau \cdot \text{iron mass/total pv})$, where 1/5 is the molar ratio of N_2/Fe^0 (Eq 6), k corrosion rate, τ the residence time.

[c] Mass flow of gas was calculated by $([N_2]_T - [N_2]_{saturation})Q$.

pressure and residence time, as was done for the field columns (Kamolpornwijit et al., 2003). However, gas production was never high enough to allow the planned experiments to be carried out. With a maximum of 4-ml trapped gas, the effect on porosity loss is ~1.5%, which exerts a negligible impact on residence time or hydraulic flow.

The column hydraulics did change, however, based on both inlet pressure monitoring (Fig. 5) and tracer test results (Fig. 6). The inlet hydrostatic pressure head fluctuated from 25 to 28 in. of water for the first 130 d; it subsequently increased and doubled the initial reading by 260 d. The increase of the pressure alone indicates a decrease in hydraulic conductivity within the Fe^0

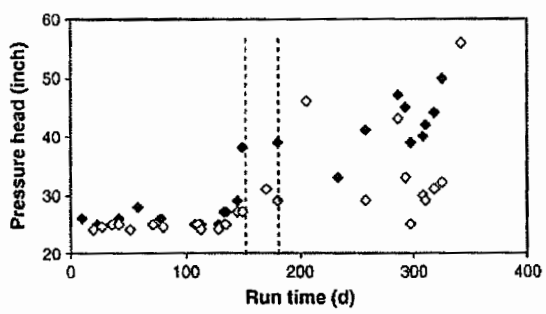

Fig. 5. Changes in inlet pressure head in the laboratory columns over time. The open (◇) and filled (◆)diamonds represent readings for columns SMC1 and SMC2, respectively. Dashed lines show a period when the effluent was recirculated back

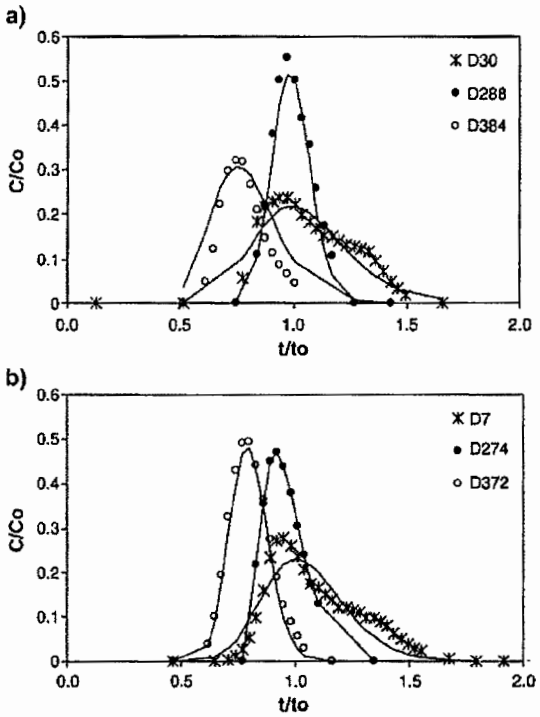

Fig. 6. Bromide tracer breakthrough curves at different run times in SMC1 (a) and SMC2 (b). Model results using CXTFIT are also plotted for the corresponding data sets.

medium. Periodic tracer tests from day 7 to 384 also show obvious changes in SMC1 (Fig. 6a) and SMC2 (Fig. 6b). The breakthrough curves obtained during early stage of the experiments (d 7 and 30) show a peak at normalized residence time of 0.95 ± 0.01, followed by a broad shoulder. This tracer tailing may be associated with the unsteady state of the system when gas production is sporadic (Reardon, 1995). The breakthrough curves obtained>100 d generally show smaller dispersion, indicating that flow was relatively homogeneous and preferential flow was absent compared with the field columns (Kamolpornwijit et al., 2003).

Using CXTFIT (Parker and van Genuchten, 1984) we modeled the breakthrough curves, and the changes in pore water velocity, column dispersivity, residence time, and effective porosity loss (Table 5). The effective porosity loss was computed as the percentage increase in pore water velocity, using the first tracer test as a baseline (For SMC1, the minimum value of pore water velocity was used). Consistent with the hydrostatic pressure build up from ~130 d onwards, pore water velocity significantly increased on d 288 in SMC1, and on d 123 in SMC2. The change in pore water velocity results from effective porosity loss, which is calculated to be $\sim 11 \pm 1\%$ around 280 d and $27 \pm 3\%$ toward the end of experiments. By then, the average residence time was 17.8 ± 0.8 h, decreased from the earlier measurements of 24.7 ± 0.2 h (Table 5).

We attribute the porosity reduction to mineral precipitation, because the hydraulic changes in the columns corresponded to the movement of the mineral precipitate front, which was visually

Table 5
Summary of CXTFIT results of the Br-tracer breakthrough curves

Day	Pore velocity (cm h^{-1})	Dispersivity (cm^2 h^{-1})	R^2	Resident time (h)	Effective porosity loss (%)
SMC1					
30	1.31	8.48E−01	0.91	23.0	0.0
108	1.22	3.78E−01	0.95	24.5	0.0
288	1.39	1.44E−01	0.97	21.6	12.1
384	1.76	9.97E−01	0.73	17.0	30.6
SMC2					
8	1.21	5.72E−01	0.87	24.9	0.0
123	1.36	1.78E−01	0.98	22.1	11.1
274	1.36	1.73E−01	0.96	22.1	10.9
372	1.61	2.67E−01	0.98	18.6	25.0

et al., 1999; Phillips et al., 2000; Wilkin et al., 2003; Kamolpornwijit et al., 2004). A rusty gelatinous precipitate formed at the sand–Fe^0 interface a day after the column operation due to fast iron oxidation by dissolved oxygen (Mackenzie et al., 1999). Within a week, gray precipitates appeared on the surface of iron grains in regions close to the inlet, similar to observation reported by Klausen et al. (2003). The gray precipitate front propagated slowly along the length of the column and reached 7 cm by 270 d. Within this 7-cm zone, additional rusty precipitates were observed by ~300 d. The extent and coloration of precipitates were the same for the two columns. By the end of the experiment the rusty precipitates appear to cover the whole ~7-cm inlet zone, which was previously occupied by the grey minerals. The gray minerals propagated further along the length of the column to ~12-cm, extending the reactive front.

The mineral precipitation at inlet sand/Fe^0 interface region was evaluated in this study as a likely cause of porosity reduction and increased average flow velocity (Liang et al., 2000; Phillips et al., 2000; Wilkin et al., 2003). The method has been described in details previously (Kamolpornwijit et al., 2004). Briefly, in the calculation of porosity loss from mineral precipitation, it is assumed that (1) all minerals precipitate uniformly throughout the column (2) Fe^0 corrodes according to the stoichiometry of NO_3^- reduction to NH_4^+ [Eq. (4)], (3) Fe^{2+} produced from Fe^0 corrosion is removed as FeOOH or Fe_3O_4 (Kamolpornwijit et al., 2004), (4) loss of dissolved Ca^{2+} is due to precipitation of $CaCO_3$, (5) the specific gravity of $CaCO_3$, FeOOH, and Fe_3O_4 are 2.93, 3.8, and 5.15, respectively (Lide, 2001). By the end of laboratory experiments (~400 pv), the porosity loss was estimated to be 8–12% of the initial porosity. Because FeOOH is less dense than Fe_3O_4 assuming FeOOH would produce a higher value of porosity loss (12%). Compared with the effective porosity loss of 25–30% derived from tracer tests (Table 5), the porosity loss estimated from uniform mineral precipitation in the columns is much lower. The difference potentially arises from the presence of immobile volume resulting from local flow diversion or blockage due to precipitation of minerals at the inlet sand/Fe^0 interface (Wilkin et al., 2003; Kamolpornwijit et al., 2004).

4. Conclusion and implications

Although it has been hypothesized that a substantial gas phase exists in Fe^0 media during groundwater treatment in a PRB, gas accumulation and entrapment in laboratory columns were

started to increase with increased biotic reduction of NO_3^- at 6–12-month run time. Based on the laboratory and field investigations we conclude that only once the microbial activity began did N_2 production become important. The chemical speciation confirms our second hypothesis: i.e., denitrification was the controlling process in gas generation of the treatment system. With an average corrosion rate of 1.7-mmol kg^{-1} d^{-1} the long-term production of N_2 is predicted to be 3.1 ml d^{-1}, which is equivalent to 1.1% pv of the laboratory columns. Gas generation alone cannot account for a substantial porosity loss (~25–30%) that was determined from tracer results in the study. The causes of the porosity loss result primarily from mineral precipitation due to enhanced corrosion by NO_3^- and a high content of Ca and alkalinity in the groundwater.

Gas production can affect Fe^0–PRB performance. Depending on the major chemical constituents in the treated water, the timing of the impact can differ (Liang et al., 2000). Without the suppressing effect of NO_3^- on oxidative action of H_2O, production of H_2 gas will occur (Reardon, 1995; Till et al., 1998; Bokermann et al., 2000). Using published data of 0.7 mmol kg^{-1} d^{-1} (Reardon, 1995) for a solution of 20-mM HCO_3^-, $H_2(g)$ production at 6.5% pv per day is predicted. The impact of $H_2(g)$ on PRB performance should happen at the start of operation when Fe^0 has the highest reactivity. This is in contrast with treatment of NO_3^- water, where N_2 gas evolves only at longer run time when microbial mediated denitrification occurs. If not effectively vented, the gas lock can significantly affect water delivery in Fe^0-medium (Birke, 2003; Vikesland et al., 2003; Bokermann, personal communication). The experimental and modeling results indicate that gas venting may be necessary in maintaining flow and the performance of PRBs, particularly for closed systems. It should be noted that the gas quantifying method is applicable only to column study with non-permeable boundaries.

Acknowledgements

We thank M. Fox for technical assistance in laboratory and field sampling. Drs. B. Gu, G.R. Moline and O.R. West provided various input to the experimental investigation. We thank Dr. C. Bokermann for his valuable discussion on gas production in granular iron. Funding for this research was supported by the Subsurface Contaminants Focus Area of the Office of Science and Technology, U.S. Department of Energy, under contract DE-AC05-00OR22725 with Oak Ridge National Laboratory, which is managed by UT-Battelle, LLC.

References

Birke, V., 2003. Mainstream and lessons learned at nine German PRB sites over 5-years—an interim report. RTDF Meeting Proceedings, Niagara Falls, New York, October 15–16, 2003.

Bokermann, C., Dahmke, A., Steiof, M., 2000. Hydrogen evolution from zero-valent iron in batch systems. Chemical Oxidation and Reactive Barriers — Remediation of Chlorinated and Recalcitrant Compounds, pp. 433–439.

Chameides, W.L., 1984. The photochemistry of a remote marine stratiform cloud. J. Geophys. Res. 89D, 4739–4755.

Cornell, R.M., Schwertmann, U., 1996. The Iron Oxides. Wiley-VCH, Weinheim.

Devlin, J.F., Eedy, R., Butler, B.J., 2002. The effects of electron donor and granular iron on nitrate transformation rates in sediments from municipal water supply aquifer. J. Contam. Hydrol. 46, 81–97.

Farrell, J., Kason, M., Melitas, N., Li, T., 2000. Investigation of the long-term performance of zero-valent iron for reductive dechlorination of trichloroethylene. Environ. Sci. Technol. 34, 514–521.

Fry, V.A., Selker, J.S., Gorelick, S.M., 1997. Experimental investigation for trapping oxygen gas in saturated porous media for in situ bioremediation. Water Resour. Res. 33 (12), 2687–2696.

Gu, B., Phelps, T.J., Liang, L., Dickey, M.J., Roh, Y., Kinsall, B.L., Palumbo, A.V., Jacobs, G.K., 1999. Biogeochemical dynamics in zero-valent iron columns: implications for permeable reactive barriers. Environ. Sci. Technol. 33,

Hansen, H.C.B., Gulberg, S., Erbs, M., Koch, C.B., 2001. Kinetics of nitrate reduction by green rusts-effects of interlayer anion and Fe(II):Fe(III) ratio. Appl. Clay Sci. 18 (1–2), 81–91.

Huang, C.P., Wang, H.W., Chiu, P.C., 1998. Nitrate reduction by metallic iron. Water Res. 32, 2257–2262.

Huang, Y.H., Zhang, T.C., Shea, P.J., Comfort, S.D., 2003. Effects of oxide coating and selected cations on nitrate reduction by iron metal. J. Environ. Qual. 32 (4), 1306–1315.

Kamolpornwijit, W., Liang, L., West, O.R., Moline, G.R., B., S.A., 2003. Heterogeneity development and its influence on long-term PRB performance: a column study. J. Contam. Hydrol. 66 (3–4), 161–178.

Kamolpornwijit, W., Moline, G.R., Liang, L., Hart, T., West, O.R., 2004. Identification and quantification of secondary mineral precipitation in Fe^0 filings from a column study. Environ. Sci. Technol. 38, 5757–5765.

Kielemoes, J., De Boever, P., Verstraete, W., 2000. Influence of denitrification on the corrosion of iron and stainless steel powder. Environ. Sci. Technol. 34 (4), 663–671.

Klausen, J., Vikesland, P.J., Kohn, T., Burris, D.R., Ball, W.P., Roberts, A.L., 2003. Longevity of granular iron in groundwater treatment processes: solution composition effects on reduction of organohalides and nitroaromatic compounds. Environ. Sci. Technol. 37, 1208–1218.

Kober, R., Schlicker, O., Ebert, M., Dahmke, A., 2002. Degradation of chlorinated ethylenes by Fe-0: inhibition processes and mineral precipitation. Environ. Geol. 41, 644–652.

Liang, L., Gu, B.H., Yin, X.P., 1996. Removal of technetium-99 from contaminated groundwater with sorbents and reductive materials. Sep. Technol. 6, 111–122.

Liang, L., Korte, N., Gu, B.H., Puls, R., Reeter, C., 2000. Geochemical and microbial reactions affecting the long-term performance of in situ 'iron barriers'. Adv. Environ. Res. 4, 273–286.

Liang, L., Moline, G., Kamolpornwijit, K., West, O.R., 2005. Influence of hydrogeochemical processes on zero-valent iron reactive barrier performance: a field investigation. J. Cont. Hydrol. 78, 291–312.

Lide, D.R., 2001. CRC Handbook of Chemistry and Physics, 81st edition. CRC Press.

Mackenzie, P.D., Horney, D.P., Sivavec, T.M., 1999. Mineral precipitation and porosity losses in granular iron columns. J. Hazard. Mater. 68, 1–17.

McIntire, G., Lippert, J., Yudelson, J., 1990. The effect of dissolved CO_2 and O_2 on the corrosion of iron. Corros. Rev. 46, 91–95.

McMahon, P.B.D.K.F., Sandstrom, M.W., 1999. Hydraulic and geochemical performance of a permeable reactive barrier containing zero-valent iron, Denver Federal Center. Ground Water 37, 396–404.

Morrison, S., 2003. Performance evaluation of a permeable reactive barrier using reaction products as tracers. Environ. Sci. Technol. 37, 2302–2309.

Morrison, S.J., Cahn, L.S., 1991. Mineralogical residence of alpha-emitting contamination and implications for mobilization from uranium mill tailings. J. Contam. Hydrol. 8, 1–21.

Parker, J.C., van Genuchten, M.Th., 1984. Determining transport parameters from laboratory and field tracer experiments. Bull. 84-3. Va. Agri. Exp. St., Blacksburg.

Phillips, D.H., Gu, B., Watson, D.B., Roh, Y., Liang, L., Lee, S.Y., 2000. Performance evaluation of a zero valent iron reactive barrier: mineralogical characteristics. Environ. Sci. Technol. 34, 4169–4176.

Reardon, E.J., 1995. Anaerobic corrosion of granular iron — measurement and interpretation of hydrogen evolution rates. Environ. Sci. Technol. 29, 2936–2945.

Scherer, M.M., Johnson, K.M., Westall, J.C., Tratnyek, P.G., 2001. Mass transport effects on the kinetics of nitrobenzene reduction by iron metal. Environ. Sci. Technol. 35, 2804–2811.

Schlicker, O., Ebert, M., Fruth, M., Weidner, M., Wust, W., Dahmke, A., 2000. Degradation of TCE with iron: the role of competing chromate and nitrate reduction. Ground Water 38, 403–409.

Stumm, V., Morgan, J.J., 1996. Aquatic Chemistry–Chemical Equilibria and Rates in Natural Waters. 3rd editionWiley-Interscience Publ., New York.

Till, B.A., Weathers, L.J., Alvarez, P.J.J., 1998. Fe(0)-supported autotrophic denitrification. Environ. Sci. Technol. 32, 634–639.

Vikesland, P.J., Klausen, J., Zimmermann, H., Roberts, A.L., Ball, W.P., 2003. Longevity of granular iron in groundwater treatment processes: changes in solute transport properties over time. J. Contam. Hydrol. 64, 3–33.

Westerhoff, P., James, J., 2003. Nitrate removal in zero-valent iron packed columns. Water Res. 37, 1818–1830.

Wilhelm, E., Battino, R., Wilcock, R.J., 1997. Low-pressure solubility of gases in liquid water. Chem. Rev. 77, 219–262.

Wilkin, R.T., Puls, R.W., Sewell, G.W., 2003. Long-term performance of permeable reactive barriers using zero-valent iron: geochemical and microbiological effects. Ground Water 41, 493–503.

Yabusaki, S., Cantrell, K., Sass, B., Steefel, C., 2001. Multicomponent reactive transport in an in situ zero-valent iron cell. Environ. Sci. Technol. 35, 1493–1503.